

Mode-coupling theory and beyond: a diagrammatic approach

Grzegorz Szamel¹

¹*Department of Chemistry, Colorado State University, Fort Collins, CO 80523, USA*

**E-mail: grzegorz.szamel@colostate.edu*

.....
For almost thirty years, mode-coupling theory has been the most widely discussed and used but also the most controversial theory of the glass transition. In this paper we briefly review the reasons for both its popularity and its controversy. We emphasize the need for the development of approaches that would be able to evaluate corrections to and extensions of the existing (standard) mode-coupling theory. Next, we review our diagrammatic formulation of the dynamics of interacting Brownian particles. We show that within this approach the standard mode-coupling theory can be derived in a very simple way. Finally, we use our diagrammatic approach to calculate two corrections to the mode-coupling theory's expression for the so-called irreducible memory function. These corrections involve re-summations of well defined classes of non-mode-coupling diagrams.
.....

Subject Index xxxx, xxx

1. Introduction

Since the publication, almost thirty years ago, of three nearly coincidental papers by Leutheusser [1], Bøtzelius, Götze and Sjölander [2], and Das, Mazenko, Ramaswamy and Toner [3], mode-coupling theory has been the most widely used and discussed, but also the most controversial theoretical approach to the glass transition problem. One reason for the popularity of this theory was that during most of the last thirty years it was the only fully microscopic theory of glassy dynamics. To be more precise, it was the only theory that, at least for particles interacting via a spherically symmetric pair-wise additive potential, allowed one to start from the microscopic description of a glassy system (*i.e.* the inter-particle interactions encoded in the pair correlation function or the static structure factor) and make predictions for dynamic quantities that can be measured in computer simulations or in real experiments. Importantly, to make these predictions the theory did not need, nor did it allow, using any fitting parameters. Thus, the mode-coupling theory was easily testable and falsifiable. For this reason, it stimulated a great number of simulational [4] and experimental [5] studies that intended to verify its predictions. Furthermore, simplified versions of the mode-coupling theory, the so-called schematic models, were found to be very useful in interpreting a variety of experimental data. These schematic models were even used to analyze systems for which the original mode-coupling theory was not intended, like molecular or polymeric fluids. Subsequently, the fully microscopic mode-coupling theory has been extended to treat some of these systems [6].

In our opinion, the most valuable tests of the mode-coupling theory were provided by computer simulations. The main reason for this is quite obvious; the same, well defined system can be used to derive theoretical predictions and to perform computer simulations. Thus, any disagreement between theory and simulations reveals an inadequacy of the theory. There is an additional reason for the usefulness of computer simulation tests of the mode-coupling theory. As we discuss below, this theory was found to describe slightly supercooled fluids. For the last twenty years the region of applicability of the mode-coupling theory was easily accessible to computer simulation studies. For these two reasons, in the following paragraphs we concentrate on the results obtained by comparing predictions of the mode-coupling theory with results of computer simulations. We refer the reader to Refs. [5, 6] for an extended comparison of theoretical and experimental results.

Simulational tests [4] of the mode-coupling theory showed that it describes rather well the initial phase of the slowing down of the fluid's dynamics upon approaching the glass transition. In particular, the theory accounts for the so-called cage effect: in a fluid approaching the glass transition a given particle spends considerable time in its solvation shell before making any significant motion. This simple physical picture of a particle's motion is reflected in a characteristic plateau in the mean-square displacement and in a two-step decay of the so-called intermediate scattering functions. Mode-coupling theory's predictions for these functions are in a good agreement with computer simulation results. In particular, we shall mention here the accuracy of the theory's predictions for the intermediate time plateau of the scattering function, which is well approximated by the so-called critical non-ergodicity parameter [7, 8], and for the time dependence in the plateau region, *i.e.* the so-called β -scale relaxation [9, 10].

The mode-coupling theory predicts that upon sufficient supercooling a fluid undergoes an ergodicity breaking transition. Furthermore, the theory predicts that upon approaching this transition the relaxation time and the self-diffusion coefficient exhibit, respectively, a power law divergence and a power law decay. Over approximately three decades of change of the relaxation time and self-diffusion coefficient, the latter predictions agree rather well with computer simulation results. To be more precise, power laws can be fitted to computer simulation results and the resulting exponents are close to those predicted by the theory. It has to be admitted, however, that the so-called mode-coupling temperature that is obtained from power law fits is usually quite different from the temperature of the ergodicity breaking transition predicted by the theory. The difference is smaller for the so-called mode-coupling volume fraction which is obtained from power law fits for hard sphere systems.

The most important negative conclusion from computer simulation studies is that the ergodicity breaking transition predicted by the mode-coupling theory is absent. Thus, for strongly supercooled fluids theoretical predictions and computer simulation results are completely different. Upon approaching the empirical mode-coupling transition point (*i.e.* the point determined by fitting procedure mentioned above), there is a crossover regime in which one observes departures of computer simulation results for the relaxation time and the self-diffusion coefficient from mode-coupling power laws. It has to be noted that until recently, standard computer simulations (excluding Monte Carlo simulations utilizing specially devised, usually non-local, moves) could only *approach* the above mentioned mode-coupling transition point. Even now, systematic studies of well equilibrated systems at and

below the mode-coupling temperature (or at and above the mode-coupling volume fraction) are quite rare.

Some of the reasons responsible for the controversy surrounding the mode-coupling theory have already been mentioned. Critics of the theory emphasize the fact that it can only describe the initial three decades of the slowing down and that it predicts a spurious (non-existent) ergodicity breaking transition. Furthermore, they point out the discrepancy between the mode-coupling temperature or volume fraction obtained from fitting the simulation results and the corresponding quantities predicted by the theory.

In addition, about fifteen years ago, it was realized that there is a very interesting phenomenon that accompanies the glass transition which cannot be described by the mode-coupling theory. A concerted simulational and experimental effort revealed that upon approaching the glass transition dynamics not only slow down but also become increasingly heterogeneous [11]. The so-called dynamic heterogeneities can be quantified in terms of four-point correlation functions that describe space and time-dependent correlations of the dynamics of individual particles. These correlation functions are very similar (although not identical) to the four-point function that is factorized in the standard derivation of the mode-coupling theory. One could argue that, since the mode-coupling theory is based upon the factorization approximation, it necessarily neglects the existence of dynamic fluctuations, it cannot describe dynamic heterogeneities, and thus constitutes a mean-field theory of the glass transition.

We should recall at this point that within a standard static mean-field theory there is an indirect way to calculate correlations (which in principle are neglected in the derivation of the mean-field equation of state). To this end one introduces an external field and shows that a susceptibility describing the change of the order parameter due to the external field diverges at the mean-field transition. Since the susceptibility can be easily related to a correlation function, in such a calculation one effectively uses a mean-field theory to reveal divergent fluctuations.

The above described standard mean-field procedure was implemented by Biroli *et al.* [12] as an inhomogeneous mode-coupling theory. Specifically, Biroli *et al.* calculated the so-called three-point susceptibility that describes the change of the intermediate scattering function (a two-point function) due to the presence of an external potential. They showed that the three-point susceptibility diverges upon approaching the ergodicity breaking transition of the mode-coupling theory. In addition, it exhibits a divergent length upon approaching this transition. This behavior of the susceptibility is quite analogous to what is found in the mean-field calculation. The analogy is somewhat incomplete in that in the standard mean-field calculation one can easily relate the divergent susceptibility to a divergent static correlation function. In contrast, the relationship of the three-point susceptibility of the inhomogeneous mode-coupling theory to any correlation function is rather unclear (and therefore a direct simulational test of inhomogeneous mode coupling theory's predictions would require a rather difficult simulational evaluation of the three-point susceptibility). In spite of this fact, Biroli *et al.*'s calculation suggests that the mode-coupling theory is indeed a mean-field theory of the glass transition.

On the other hand, results of recent mode-coupling calculations and computer simulations in higher spatial dimensions raised some doubts about the mean-field character of the mode-coupling theory. The reason for this is that this theory does not seem to become more accurate in higher spatial dimension, which is a behavior that one would expect of a mean-field theory. First, it was showed [13, 14] that for hard spheres in high spatial dimensions the ergodicity breaking transition volume fraction predicted by the mode-coupling theory lies above the so-called dynamic transition volume fraction and even above the Kauzmann transition volume fraction which are predicted by a static replica theory [15, 16]. Since the latter theory also aspires to be a mean-field theory of the glass transition, the difference between these predictions is rather disconcerting and suggests that at least one of these theories may be incorrect. Moreover, as pointed out by Ikeda and Miyazaki [14], in higher spatial dimensions, the long time limit of the self part of the van Hove function at the mode-coupling transition develops unphysical negative tails. Finally, results of recent computer simulations studies [17] in higher spatial dimensions seem to be consistent with the replica approach and, therefore, suggest that the mode-coupling theory might not be a correct mean-field theory of the glass transition. In our opinion more work is needed to fully resolve this issue.

Somewhat surprisingly, during most of the thirty years of the existence of the mode-coupling theory, relatively little work has been done on the investigation of its most fundamental approximation, *i.e.* the factorization approximation, and on the development of extensions and improvements of the theory. In our opinion this was, in part, due to the original derivation of the most widely applied version of the theory, which was reviewed in details in Refs. [6, 18]. This derivation, while well suited to obtain rather quickly the mode-coupling equations, is an inconvenient starting point for calculating corrections to the standard theory. It is only relatively recently that several alternative, diagrammatic derivations of the mode-coupling theory have been proposed [19–21]. Notably, most of these derivations are quite complicated. Thus, it is not clear whether they could be used to calculate corrections to the mode-coupling theory.

We mention here two related but different attempts to derive extensions of the standard mode-coupling theory, which were proposed shortly after the original theory was derived. Das and Mazenko [22] showed that the sharp ergodic-nonergodic transition that Ref. [3] predicted is cut off if, in addition to the mode-coupling diagrams, one also includes diagrams that enforce the standard relationship between the momentum density, the particle density and the velocity field. At almost the same time Götze and Sjögren [23] showed that the transition predicted by the version of the theory proposed in Ref. [2] is cut off due to coupling to current modes. Subsequently, it was argued that the latter cut off should be understood as a hopping or an activated process.

Recently, these two approaches, and related ones presented later in Refs. [24, 25], were criticized by Cates and Ramaswamy [26]. These authors argued in quite general terms that couplings to current modes result in negligible contributions and cannot induce hopping or activated processes.

We shall mention here that there is another reason why coupling to current modes cannot constitute a universal extension of mode-coupling theory which cuts off the spurious transition and cures other problems of this theory. The reason is that the long-time dynamics of systems in which the underlying (microscopic) dynamics is Brownian is surprisingly similar

to that of systems evolving with Newtonian dynamics. It has been known for some time that at the level of the standard mode-coupling approximation Brownian and Newtonian microscopic dynamics result in the same glass transition scenario [27]. Later, it was showed using computer simulations that deviations from the mode-coupling-like behavior are the same in systems with stochastic dynamics and Newtonian dynamics [28] and in systems with Brownian dynamics and Newtonian dynamics [29]. The implication of these studies is that the mechanism that cuts off the spurious transition predicted by the mode-coupling theory is likely the same in systems with different microscopic dynamics. Since in systems with Brownian dynamics current modes cannot be defined (at least not in the same way as in systems with Newtonian dynamics), the mechanism introduced in Refs. [22–24] cannot operate there.

Finally, we shall also mention here the so-called generalized mode-coupling approach. This line of research was started when we recognized [30] that by moving mode-coupling theory’s factorization approximation to a higher level correlation function the location of the ergodicity breaking transition predicted by the theory can be moved towards the empirical transition determined by fitting simulational data to mode-coupling-like power laws. Subsequently, Wu and Cao [31] extended our calculation and showed that by moving the factorization approximation by two levels one can get even better agreement between theory and simulations. Finally, Mayer *et al.* [32] showed at the level of a schematic model that if one avoids the factorization approximation altogether, the resulting theory does not have a spurious ergodicity breaking transition. On the one hand, this development looks quite promising. We showed [33], however, that from the diagrammatic point of view, the generalized mode-coupling theory re-sums fewer diagrams than the standard mode-coupling theory. It is known in the liquid state theory that re-summing more diagrams does not always result in a more accurate theory. It would, however, be more satisfactory to correct mode-coupling approach by adding diagrams that describe dynamic events that are neglected in the standard mode-coupling approach.

In the reminder of this paper we will review our diagrammatic formulation [34] of the dynamics of strongly interacting systems of Brownian particles. We will show that this approach can be used to derive, in a rather straightforward way, the standard version of the mode-coupling theory. Finally, we will show that it can also be used to incorporate dynamic events that are neglected in the standard theory. Specifically, we will evaluate the simplest corrections to the mode-coupling theory’s expression for the so-called irreducible memory function.

2. Diagrammatic approach

2.1. Derivation

We consider a system of N interacting Brownian particles in a volume V . The average density is $n = N/V$. The brackets $\langle \dots \rangle$ indicate a canonical ensemble average at a temperature T . As shown in Ref. [34], after some preliminary calculations it is convenient to take the thermodynamic limit, $N \rightarrow \infty, V \rightarrow \infty, N/V = n = \text{const.}$

We define the time dependent equilibrium correlation function of the Fourier components of the microscopic density as

$$\langle n(\mathbf{k}_1; t) n^*(\mathbf{k}_2) \rangle, \quad (1)$$

with $n(\mathbf{k}_1; t)$ being the Fourier transform of the microscopic density fluctuation at a time t ,

$$n(\mathbf{k}_1; t) = \sum_{j=1}^N e^{-i\mathbf{k}_1 \cdot \mathbf{r}_j(t)} - \left\langle \sum_{j=1}^N e^{-i\mathbf{k}_1 \cdot \mathbf{r}_j} \right\rangle, \quad (2)$$

and $n(\mathbf{k}_2) \equiv n(\mathbf{k}_2; t=0)$. In a diagrammatic series it is convenient to express the density correlation function in terms of the so-called response function $G(k; t)$,

$$\theta(t) \langle n_1(\mathbf{k}_1; t) n_1^*(\mathbf{k}_2) \rangle = nG(k; t) S(k) (2\pi)^3 \delta(\mathbf{k}_1 - \mathbf{k}_2). \quad (3)$$

Note that due to the translational invariance, the correlation function $\langle n_1(\mathbf{k}_1; t) n_1^*(\mathbf{k}_2) \rangle$ is diagonal in wave-vector space. The response function is related to the usual collective intermediate scattering function $F(k; t)$,

$$F(k; t) = G(k; t) S(k). \quad (4)$$

To derive the diagrammatic series for the response function G it is convenient to start from a hierarchy of equations of motion for the correlation functions of orthogonalized densities. The first such correlation function coincides with formula (1). The second one,

$$\langle n_2(\mathbf{k}_1, \mathbf{k}_2; t) n^*(\mathbf{k}_3) \rangle, \quad (5)$$

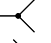
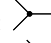
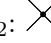
is a correlation function of the part of the two-particle density fluctuation that is orthogonal to the density fluctuation, $n_2(\mathbf{k}_1, \mathbf{k}_2; t)$,

$$\begin{aligned} n_2(\mathbf{k}_1, \mathbf{k}_2; t) &= \sum_{i \neq j=1}^N e^{-i\mathbf{k}_1 \cdot \mathbf{r}_i(t) - i\mathbf{k}_2 \cdot \mathbf{r}_j(t)} - \left\langle \sum_{i \neq j=1}^N e^{-i\mathbf{k}_1 \cdot \mathbf{r}_i - i\mathbf{k}_2 \cdot \mathbf{r}_j} \right\rangle \\ &\quad - \sum_{\mathbf{q}_1, \mathbf{q}_2} \left\langle \sum_{i \neq j=1}^N e^{-i\mathbf{k}_1 \cdot \mathbf{r}_i - i\mathbf{k}_2 \cdot \mathbf{r}_j} n^*(\mathbf{q}_1) \right\rangle \langle n(\mathbf{q}_1) n^*(\mathbf{q}_2) \rangle^{-1} n(\mathbf{q}_2; t), \end{aligned} \quad (6)$$

and the density fluctuation $n(\mathbf{k}_3)$. One should note that by definition $\langle n_2(\mathbf{k}_1, \mathbf{k}_2; t=0) n^*(\mathbf{k}_3) \rangle = 0$.

We shall mention here that the orthogonalized densities were introduced before [35, 36] in the context of a diagrammatic approach to the dynamics of Newtonian systems. The advantage of describing the system in terms of correlation functions of orthogonalized densities is two-fold. First, the introduction of the orthogonalized densities allows us to avoid having additional, rather unusual, diagrams that impose the equilibrium distribution at the initial time. Technically, this follows from the vanishing of all higher order correlation at $t=0$, $\langle n_l(\mathbf{k}_1, \dots, \mathbf{k}_l; t=0) n^*(\mathbf{k}_{l+1}) \rangle = 0$. Second, if equations of motion are written in terms of the correlation functions of orthogonalized densities, the bare inter-particle interactions are automatically renormalized. Specifically, in the equations of motions the inter-particle potential is replaced by combinations of equilibrium correlation functions. The disadvantage of using orthogonalized densities is that in addition to equilibrium pair correlations, many-particle correlations are needed to express renormalized interactions. To make our approach tractable we perform a cluster expansion of the renormalized interactions and neglect terms involving higher order equilibrium correlations. While this approximation is implicit in all recent diagrammatic approaches to the dynamics of strongly interacting fluids, its consequences have yet to be investigated.

As shown in Ref. [34], the hierarchy of equations of motion for the correlation functions of orthogonalized densities can be replaced by a hierarchy of integral equations involving the same functions. The latter hierarchy can be solved by iteration for the response function (3) and the resulting expressions can be represented in terms of diagrams. The diagrams consist of the following elements:

- response function $G(k; t)$: \xleftarrow{k}
- bare response function $G_0(k; t)$: \xleftarrow{k}
- “left” vertex \mathcal{V}_{12} : 
- “right” vertex \mathcal{V}_{21} : 
- four-leg vertex \mathcal{V}_{22} : 

The bare response function $G_0(k; t)$ is defined as

$$G_0(k; t) = \theta(t) \exp(-D_0 k^2 t / S(k)), \quad (7)$$

and the explicit expressions for the three- and four-leg vertices are:

$$\mathcal{V}_{12}(\mathbf{k}_1; \mathbf{k}_2, \mathbf{k}_3) = D_0 (2\pi)^3 \delta(\mathbf{k}_1 - \mathbf{k}_2 - \mathbf{k}_3) k_1 v_{\mathbf{k}_1}(\mathbf{k}_2, \mathbf{k}_3) \quad (8)$$

$$\mathcal{V}_{21}(\mathbf{k}_1, \mathbf{k}_2; \mathbf{k}_3) = n D_0 (2\pi)^3 \delta(\mathbf{k}_1 + \mathbf{k}_2 - \mathbf{k}_3) S(k_1) S(k_2) k_3 v_{\mathbf{k}_3}(\mathbf{k}_1, \mathbf{k}_2) S(k_3)^{-1}, \quad (9)$$

$$\begin{aligned} \mathcal{V}_{22}(\mathbf{k}_1, \mathbf{k}_2; \mathbf{k}_3, \mathbf{k}_4) = \\ n D_0 (2\pi)^3 S(k_1) S(k_2) \delta(\mathbf{k}_1 + \mathbf{k}_2 - \mathbf{k}_3 - \mathbf{k}_4) \mathbf{v}(\mathbf{k}_1, \mathbf{k}_2) \cdot \mathbf{v}(\mathbf{k}_3, \mathbf{k}_4) \end{aligned} \quad (10)$$

In Eqs. (8-9), vertices \mathcal{V}_{12} and \mathcal{V}_{21} are expressed in terms of the following function,

$$v_{\mathbf{k}_1}(\mathbf{k}_2, \mathbf{k}_3) = \hat{\mathbf{k}}_1 \cdot (c(k_2)\mathbf{k}_2 + c(k_3)\mathbf{k}_3). \quad (11)$$

In the literature, $v_{\mathbf{k}_1}(\mathbf{k}_2, \mathbf{k}_3)$ is referred to as the vertex function of the mode-coupling theory. Furthermore, in Eq. (10), vertex \mathcal{V}_{22} is expressed in terms of a similar function,

$$\mathbf{v}(\mathbf{k}_1, \mathbf{k}_2) = c(k_1)\mathbf{k}_1 + c(k_2)\mathbf{k}_2. \quad (12)$$

In later sections we will also use the following functions related to v and \mathbf{v} ,

$$\tilde{v}_{\mathbf{k}_1}(\mathbf{k}_2, \mathbf{k}_3) = \hat{\mathbf{k}}_1 \cdot (c(k_2)\mathbf{k}_2 + c(k_3)\mathbf{k}_3) / k_1, \quad (13)$$

$$\tilde{\mathbf{v}}(\mathbf{k}_1, \mathbf{k}_2) = (c(k_1)\mathbf{k}_1 + c(k_2)\mathbf{k}_2) / |\mathbf{k}_1 + \mathbf{k}_2|. \quad (14)$$

In the diagrams contributing to the response function, we refer to the leftmost bare response function as the left root, and to the other bare response functions as bonds. The left root is labeled by a wave-vector and the bonds are unlabeled. We consider two diagrams to be topologically equivalent if there is a way to assign labels to unlabeled bonds so that the resulting labeled diagrams are topologically equivalent¹. To evaluate an unlabeled diagram one assigns wave-vectors to unlabeled bonds, integrates over all wave-vectors (with a $(2\pi)^{-3}$ factor for each integration) except the wave-vector corresponding to the left root, integrates over all intermediate times, and divides the result by a symmetry number of the diagram (*i.e.*

¹ Two labeled diagrams are topologically equivalent if each labeled bond in one diagram connects vertices of the same type as the corresponding labeled bond in the other diagram [37].

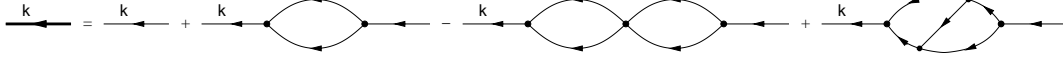


Fig. 1 Diagrammatic series expansion for response function $G(k; t)$ [34].

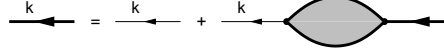


Fig. 2 Diagrammatic representation of the Dyson equation, Eq. (16) [34].

the number of topologically identical labeled diagrams that can be obtained from a given unlabeled diagram by permutation of the bond labels).

As showed in Ref. [34], the response function given by the following series:

$$G(k; t) = \quad (15)$$

sum of all topologically different diagrams with a left root labeled k , a right root, G_0 bonds, \mathcal{V}_{12} , \mathcal{V}_{21} and \mathcal{V}_{22} vertices, in which diagrams with odd and even numbers of \mathcal{V}_{22} vertices contribute with overall negative and positive sign, respectively.

The first few diagrams contributing to the series (15) are shown in Fig. 1.

2.2. Memory functions: reducible and irreducible

We should emphasize that our diagrammatic expansion was not derived from a field-theoretical approach. However, once a diagrammatic approach has been derived, we can use re-arrangements and re-summations that were originally introduced in the context of field-theoretical diagrammatic expansions. In particular, we can write down a Dyson equation in the usual form,

$$G(k; t) = G_0(k; t) + \int_0^t dt_1 \int_0^{t_1} dt_2 \int \frac{d\mathbf{k}_1}{(2\pi)^3} G_0(k; t - t_1) \Sigma(\mathbf{k}, \mathbf{k}_1; t_1 - t_2) G(k_1; t_2). \quad (16)$$

Here Σ is the self-energy. The diagrammatic representation of the Dyson equation is showed in Fig. 2. Due to the translational invariance the self-energy is diagonal in the wave-vector space,

$$\Sigma(\mathbf{k}, \mathbf{k}_1; t) \propto (2\pi)^3 \delta(\mathbf{k} - \mathbf{k}_1). \quad (17)$$

It can be showed from the Dyson equation that the self-energy Σ is a sum of diagrams that do not separate into disconnected components upon removal of a single bond. To make a connection with the projection operator-based approach [27, 38] we need to relate the self-energy to a memory function. First, we note that the diagrams contributing to the self-energy start with \mathcal{V}_{21} vertex on the right and end with \mathcal{V}_{12} vertex on the left. It turns out that in order to relate the self-energy to a memory function for a Brownian system, we need to factor out parts of these vertices. First, we define a memory matrix \mathbf{M} by factoring out \mathbf{k} from the

left vertex and $(D_0/S(k_1))\mathbf{k}_1$ from the right vertex,

$$\Sigma(\mathbf{k}, \mathbf{k}_1; t) = D_0 \mathbf{k} \cdot \mathbf{M}(\mathbf{k}, \mathbf{k}_1; t) \cdot \mathbf{k}_1 S(k_1)^{-1}. \quad (18)$$

Due to translational invariance the memory matrix \mathbf{M} is diagonal in the wave-vector space. Moreover, only its longitudinal component contributes to the self-energy. Thus, we can define the memory function M through the following relation

$$\hat{\mathbf{k}} \cdot \mathbf{M}(\mathbf{k}, \mathbf{k}_1; t) \cdot \hat{\mathbf{k}} = M(k; t) (2\pi)^3 \delta(\mathbf{k} - \mathbf{k}_1). \quad (19)$$

Using Eqs. (18) and (19) in the Laplace transform of the Dyson equation, we can obtain the following equation,

$$G(k; z) = G_0(k; z) + G_0(k; z) \frac{D_0 k^2}{S(k)} M(k; z) G(k; z). \quad (20)$$

Eq. (20) can be solved with respect to (w.r.t.) response function $G(k; z)$. Using the definition of bare response function G_0 we obtain

$$G(k; z) = \frac{1}{z + \frac{D_0 k^2}{S(k)} (1 - M(k; z))}. \quad (21)$$

Multiplying both sides of the above equation by the static structure factor and using the relation (4) between G and the intermediate scattering function F we get the standard memory function representation [38] of the intermediate scattering function,

$$F(k; z) = \frac{S(k)}{z + \frac{D_0 k^2}{S(k)} (1 - M(k; z))}. \quad (22)$$

The memory function representation (22) is the first step in the derivation of the mode-coupling equations that utilizes the projection operator formalism.

To analyze the diagrams contributing to the memory matrix it is convenient to introduce cut-out vertices:

$$\mathbf{V}_{12}^c(\mathbf{k}_1; \mathbf{k}_2, \mathbf{k}_3) = D_0 (2\pi)^3 \delta(\mathbf{k}_1 - \mathbf{k}_2 - \mathbf{k}_3) (c(k_2)\mathbf{k}_2 + c(k_3)\mathbf{k}_3) \quad (23)$$

$$\mathbf{V}_{21}^c(\mathbf{k}_1, \mathbf{k}_2; \mathbf{k}_3) = n (2\pi)^3 \delta(\mathbf{k}_1 + \mathbf{k}_2 - \mathbf{k}_3) S(k_1) S(k_2) (c(k_1)\mathbf{k}_1 + c(k_2)\mathbf{k}_2). \quad (24)$$

These vertices are obtained by factoring out \mathbf{k}_1 from vertex \mathcal{V}_{12} and $(D_0/S(k_3))\mathbf{k}_3$ from vertex \mathcal{V}_{21} (one should note that the same factorization was used in the definition of the memory matrix in Eq. (18)).

It should be noted that

$$\mathcal{V}_{22}(\mathbf{k}_1, \mathbf{k}_2; \mathbf{k}_3, \mathbf{k}_4) = \int \frac{d\mathbf{k}'}{(2\pi)^3} \mathbf{V}_{21}^c(\mathbf{k}_1, \mathbf{k}_2; \mathbf{k}') \cdot \mathbf{V}_{12}^c(\mathbf{k}'; \mathbf{k}_3, \mathbf{k}_4). \quad (25)$$

The diagrammatic rules for functions \mathbf{V}_{12}^c and \mathbf{V}_{21}^c are as follows:

- “left” cut-out vertex \mathbf{V}_{12}^c : \leftarrow
- “right” cut-out vertex \mathbf{V}_{21}^c : \rightarrow

and we refer to wave-vector \mathbf{k}_1 in $\mathbf{V}_{12}^c(\mathbf{k}_1; \mathbf{k}_2, \mathbf{k}_3)$ and \mathbf{k}_3 in $\mathbf{V}_{21}^c(\mathbf{k}_1, \mathbf{k}_2; \mathbf{k}_3)$ as roots of these vertices. Note that to evaluate a diagram contributing to the memory matrix we do not integrate over either left or right roots.

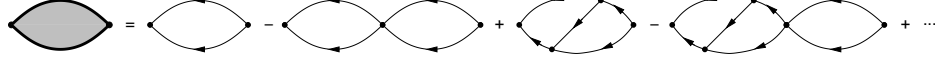


Fig. 3 Diagrammatic series expansion for memory matrix \mathbf{M} .



Fig. 4 Memory matrix \mathbf{M} can be represented as a sum of \mathbf{M}^{irr} and all other diagrams [34]. The latter diagrams can be re-summed and it is easy to see that as a result we get the second diagram at the right-hand side.

It follows from the definition of the memory matrix \mathbf{M} that

$$\mathbf{M}(\mathbf{k}, \mathbf{k}_1; t) = \quad (26)$$

sum of all topologically different diagrams which do not separate into disconnected components upon removal of a single bond, with vertex \mathbf{V}_{12}^c with root \mathbf{k} on the left and vertex \mathbf{V}_{21}^c with root \mathbf{k}_1 on the right, G_0 bonds, \mathcal{V}_{12} , \mathcal{V}_{21} and \mathcal{V}_{22} vertices, in which diagrams with odd and even numbers of \mathcal{V}_{22} vertices contribute with overall negative and positive sign, respectively.

The first few diagrams in the series for \mathbf{M} are showed in Fig. 3.

The series expansion for \mathbf{M} consists of diagrams that are one-propagator irreducible (*i.e.* diagrams that do not separate into disconnected components upon removal of a single bond). However, not all of these diagrams are completely one-particle irreducible. Specifically, some of the diagrams contributing to \mathbf{M} separate into disconnected components upon removal of a \mathcal{V}_{22} vertex. In analogy with terminology used in the context of Mayer diagrams, we will call such a vertex an articulation \mathcal{V}_{22} vertex or articulation four-leg vertex. The examples of diagrams containing one articulation \mathcal{V}_{22} vertex are the second and the fourth diagrams on the right-hand side of the diagrammatic equation showed in Fig. 3. Intuitively, it is clear that the series (26) can be further re-arranged by writing down a second Dyson-type equation. In the projection operator formalism, this second Dyson-type equation corresponds to the equation that defines the so-called irreducible memory function [27, 39, 40] in terms of the memory function defined through Eq. (19).

In the diagrammatic approach, we define the irreducible memory matrix \mathbf{M}^{irr} as a sum of only those diagrams in the series for \mathbf{M} that do not separate into disconnected components upon removal of a single \mathcal{V}_{22} vertex. To distinguish memory matrix \mathbf{M} from the irreducible matrix \mathbf{M}^{irr} we will sometimes use the term reducible memory matrix when referring to \mathbf{M} . We will also sometimes use the term reducible memory function when referring to M defined in Eq. (19).

Diagrammatically, we can represent memory matrix \mathbf{M} as a sum of \mathbf{M}^{irr} and all other diagrams. The latter diagrams can be re-summed as showed in Fig. 4. Using Eq. (25), we can introduce an additional integration over a wave-vector and then we see that the diagrammatic

equation showed in Fig. 4 corresponds to the following equation,

$$\mathbf{M}(\mathbf{k}, \mathbf{k}_1; t) = \mathbf{M}^{\text{irr}}(\mathbf{k}, \mathbf{k}_1; t) - \int_0^t dt_1 \int \frac{d\mathbf{k}_2}{(2\pi)^3} \mathbf{M}^{\text{irr}}(\mathbf{k}, \mathbf{k}_2; t - t_1) \cdot \mathbf{M}(\mathbf{k}_2, \mathbf{k}_1; t_1) \quad (27)$$

Again, we use translational invariance and then introduce the irreducible memory function M^{irr} as the longitudinal component of the matrix \mathbf{M}^{irr} ,

$$\hat{\mathbf{k}} \cdot \mathbf{M}^{\text{irr}}(\mathbf{k}, \mathbf{k}_1; t) \cdot \hat{\mathbf{k}} = M^{\text{irr}}(k; t)(2\pi)^3 \delta(\mathbf{k} - \mathbf{k}_1), \quad (28)$$

Then, the longitudinal component of the Laplace transform of Eq. (27) can be written in the following way

$$M(k; z) = M^{\text{irr}}(k; z) - M^{\text{irr}}(k; z)M(k; z). \quad (29)$$

This equation can be solved w.r.t. memory function M . Substituting the solution into Eq. (22) we obtain a representation of the intermediate scattering function in terms of the irreducible memory function,

$$F(k; z) = S(k)G(k; z) = \frac{S(k)}{z + \frac{D_0 k^2}{S(k)(1+M^{\text{irr}}(k; z))}}. \quad (30)$$

Eq. (30) was first derived by Cichocki and Hess [39] using a projection operator approach. Subsequently, it was used by Szamel and Löwen [27] to derive the standard mode-coupling theory for Brownian systems.

Diagrammatically,

$$\mathbf{M}^{\text{irr}}(\mathbf{k}, \mathbf{k}_1; t) = \quad (31)$$

sum of all topologically different diagrams which do not separate into disconnected components upon removal of a single bond or a single \mathcal{V}_{22} vertex, with vertex \mathbf{V}_{12}^c with root \mathbf{k} on the left and vertex \mathbf{V}_{21}^c with root \mathbf{k}_1 on the right, G_0 bonds, \mathcal{V}_{12} , \mathcal{V}_{21} and \mathcal{V}_{22} , in which diagrams with odd and even numbers of \mathcal{V}_{22} vertices contribute with overall negative and positive sign, respectively.

The first few diagrams in the series for \mathbf{M}^{irr} are shown in Fig. 5. We will analyze three classes of these diagrams in the following sections. Here we will only notice that the first diagram at the right-hand-side of the diagrammatic equation showed in Fig. 5 separates into two disconnected pieces upon removal of the left and right vertices. The remaining three diagrams do not share this property. We shall point out the important difference between the second and third diagrams and the fourth diagram. The latter diagram is two-line-reducible, *i.e.* it separates into two disconnected pieces upon removing the left and right vertices and cutting through two propagator lines (note that each of these pieces contains at least two horizontal lines and is itself internally connected). Roughly speaking, the fourth diagram has the the same nontrivial part as the second diagram but iterated twice. In contrast, the second and third diagrams are two-line-irreducible: upon removing the left and right vertices they cannot be separated into two internally connected pieces by cutting through two propagator lines.

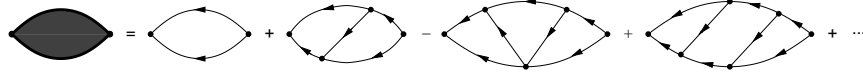


Fig. 5 Diagrammatic series expansion for the irreducible memory matrix \mathbf{M}^{irr} .



Fig. 6 Re-summation of diagrams that separate into two disconnected components upon removal of the \mathbf{V}_{12}^c and \mathbf{V}_{21}^c vertices leads to a one-loop diagram with G bonds [34].

3. Standard mode-coupling approximation

To obtain the standard mode-coupling expression for the memory function it is convenient to start from a series expression for \mathbf{M}^{irr} showed in Fig. 5. The simplest re-summation of this series includes diagrams that separate into two disconnected components upon removal of the left, \mathbf{V}_{12}^c , and the right, \mathbf{V}_{21}^c , vertices. Out of the diagrams at the right-hand-side of the diagrammatic equation showed in Fig. 5, this re-summation includes only the first diagram. We will call diagrams that separate into two disconnected components upon removal of the left and right vertices mode-coupling diagrams.

In the diagrams included in the present re-summation, each of the two components that appear after removing the left and right vertices is a part of the series for the response function G . Thus, the present re-summation results in a one-loop diagram (*i.e.* the first diagram shown on the right-hand side in Fig. 5) with bare G_0 bonds replaced by G bonds, see Fig. 6. Thus, we get a self-consistent one-loop approximation for the memory matrix,

$$\mathbf{M}^{\text{irr}}(\mathbf{k}, \mathbf{k}_1; t) \approx \mathbf{M}_{\text{one-loop}}^{\text{irr}}(\mathbf{k}, \mathbf{k}_1; t) = \frac{1}{2} \int \frac{d\mathbf{k}_2 d\mathbf{k}_3}{(2\pi)^6} \mathbf{V}_{12}^c(\mathbf{k}; \mathbf{k}_2, \mathbf{k}_3) G(k_2; t) G(k_3; t) \mathbf{V}_{21}^c(\mathbf{k}_2, \mathbf{k}_3; \mathbf{k}_1). \quad (32)$$

The overall factor $1/2$ reflects the symmetry number of the one-loop diagram, which is equal to 2.

Using explicit expressions (23-24) for the cut-out vertices we show that (32) leads to the following expression for the irreducible memory function (recall that the irreducible memory function is obtained from the memory matrix by using translational invariance and taking the matrix's longitudinal component):

$$M^{\text{irr}}(k; t) \approx M_{\text{one-loop}}^{\text{irr}}(k; t) = \frac{nD_0}{2} \int \frac{d\mathbf{k}_1}{(2\pi)^3} v_{\mathbf{k}}^2(\mathbf{k}_1, \mathbf{k} - \mathbf{k}_1) S(k_1) S(|\mathbf{k} - \mathbf{k}_1|) G(k_1; t) G(|\mathbf{k} - \mathbf{k}_1|; t) \equiv M_{\text{MCT}}^{\text{irr}}(k; t) \quad (33)$$

where $v_{\mathbf{k}}(\mathbf{k}_1, \mathbf{k} - \mathbf{k}_1)$ denotes the so-called mode-coupling theory's vertex defined in Eq. (11). As indicated in Eq. (33), the self-consistent one-loop approximation coincides with the standard mode-coupling approximation, *i.e.* both approximations result in exactly the same expression for the irreducible memory function. By combining the memory function representation (30) with the standard mode-coupling approximation for the memory function (33), one can derive existence and analyze the properties of an ergodicity breaking transition.

More generally, if one assumes that at a certain state point the response function acquires a non-vanishing long-time limit,

$$\lim_{t \rightarrow \infty} G(k; t) = f(k), \quad (34)$$

where f is referred to as a non-ergodicity parameter, using Eqs. (30) one can derive the well known equation for f ,

$$\frac{f(k)}{1 - f(k)} = m(k). \quad (35)$$

In Eq. (35), $m(k)$ is related to the long-time limit of the irreducible memory function,

$$m(k) = \lim_{t \rightarrow \infty} \frac{S(k)}{D_0 k^2} M^{\text{irr}}(k; t). \quad (36)$$

It should be emphasized that Eqs. (35-36) are independent of the mode-coupling approximation and, in fact, are exact. Specifically, if the response function does not decay, its long-time limit is connected to the long-time limit of the memory function via Eqs. (35-36).

Within the standard mode-coupling approximation m is given by

$$m(k) \approx m_{\text{MCT}}(k) = \frac{nS(k)}{2} \int \frac{d\mathbf{k}_1}{(2\pi)^3} \tilde{v}_{\mathbf{k}}^2(\mathbf{k}_1, \mathbf{k} - \mathbf{k}_1) S(k_1) S(|\mathbf{k} - \mathbf{k}_1|) f(k_1) f(|\mathbf{k} - \mathbf{k}_1|), \quad (37)$$

where we used a modified vertex function \tilde{v} defined in Eq. (13).

4. Two corrections to the standard mode-coupling approximation

4.1. General considerations

To improve upon the standard mode-coupling approximation we need to include at least some of the diagrams that are neglected in the re-summation leading to the self-consistent one-loop approximation for the memory matrix. For example, we might include some or all of 2nd, 3rd, or 4th diagrams at the right-hand-side of the diagrammatic equation showed in Fig. 5. We will refer to such diagrams, *i.e.* to diagrams contributing to the irreducible memory matrix which do not separate into disconnected components upon removing the left and right vertices, as non-mode-coupling diagrams.

The simplest non-mode-coupling diagram is the 2nd diagram showed at the right-hand-side of the diagrammatic equation in Fig. 5. Of course, including just the “bare” 2nd diagram (*i.e.* including the 2nd diagram with G_0 bonds) would only introduce a trivial change of the irreducible memory function. Instead, one should try to perform a re-summation of the diagrams with the same “skeleton” as the 2nd diagram at the right-hand-side in Fig. 5. Specifically, one could try to sum all diagrams that can be obtained from the 2nd diagram at the right-hand-side in Fig. 5 by replacing the bare response functions G_0 by diagrams that appear in the diagrammatic expansion for the full response function, Eq. (15). Such replacements will be referred to as response function-like insertions. The re-summation of the 2nd diagram at the right-hand-side in Fig. 5 with all possible response function-like insertions would result in the same diagram, but with the bare response functions G_0 replaced by the full response functions G , see Fig. 7.

In general, such re-summations look quite promising. A possible strategy would be to include at least some non-mode-coupling diagrams or perhaps a class of non-mode-coupling



Fig. 7 Re-summation of diagrams that can be obtained from the 2nd diagram at the right-hand-side in Fig. 5 by replacing the bare response functions G_0 by diagrams that appear in the diagrammatic expansion for the full response function, Eq. (15), gives the same diagram but with G bonds.

diagrams, with an implicit re-summation of all possible response function-like insertions, and to use the resulting expression to calculate the correction to the mode-coupling (*i.e.* self-consistent one-loop) approximation for the irreducible memory function. An obvious possible pitfall is double-counting some contributions. A less obvious pitfall is that one can quite easily generate spurious, non-physical long-time divergences. In fact, the diagram showed in Fig. 7 provides an example of such a divergence. The origin of the divergence is that this diagram has unrestricted integrations over intermediate times. This divergence is discussed in the remainder of the present subsection. In the next subsection, Sec. 4.2, we show that by combining the diagram showed in Fig. 7 with other similar diagrams this unphysical divergence can be avoided.

The diagram showed in Fig. 7 leads to the following contribution to the irreducible memory function (the contribution to the irreducible memory function is obtained from the diagram showed in Fig. 7 by using translational invariance and taking the longitudinal component of the expression corresponding to this diagram, see Eq. (28)):

$$\begin{aligned} \delta M_0^{\text{irr}}(k; t) = & n^2 D_0^3 \int_0^t dt_2 \int_0^{t_2} dt_1 \int \frac{d\mathbf{k}_1 d\mathbf{k}_2}{(2\pi)^6} v_{\mathbf{k}}(\mathbf{k}_1 + \mathbf{k}_2, \mathbf{k} - \mathbf{k}_1 - \mathbf{k}_2) \\ & \times G(|\mathbf{k}_1 + \mathbf{k}_2|; t - t_2) |\mathbf{k}_1 + \mathbf{k}_2| v_{\mathbf{k}_1 + \mathbf{k}_2}(\mathbf{k}_1, \mathbf{k}_2) G(|\mathbf{k} - \mathbf{k}_1 - \mathbf{k}_2|; t - t_1) S(|\mathbf{k} - \mathbf{k}_1 - \mathbf{k}_2|) \\ & \times G(k_2; t_2 - t_1) S(k_2) v_{\mathbf{k} - \mathbf{k}_1}(\mathbf{k} - \mathbf{k}_1 - \mathbf{k}_2, \mathbf{k}_2) |\mathbf{k} - \mathbf{k}_1| G(|\mathbf{k} - \mathbf{k}_1|; t_1) G(k_1; t_2) S(k_1) \\ & \times v_{\mathbf{k}}(\mathbf{k}_1, \mathbf{k} - \mathbf{k}_1). \end{aligned} \quad (38)$$

Note that factors $|\mathbf{k}_1 + \mathbf{k}_2|$ and $|\mathbf{k} - \mathbf{k}_1|$ originate from the definition of the vertices, Eqs. (8-9). Similar factors will appear below in Eqs. (40) and (45).

One can show that if the full response function G develops a long-lived plateau, the contribution to the irreducible memory function given by the diagram showed in Fig. 7 grows with time rather than exhibits a plateau. In particular, if the full response function acquires a non-vanishing long time limit, $\lim_{t \rightarrow \infty} G(k; t) = f(k)$, the contribution to the irreducible memory function resulting from the diagram showed in Fig. 7 diverges as t^2 as t increases:

$$\begin{aligned} \delta M_0^{\text{irr}}(k; t) = & \frac{1}{2} t^2 n^2 D_0^3 \int \frac{d\mathbf{k}_1 d\mathbf{k}_2}{(2\pi)^6} v_{\mathbf{k}}(\mathbf{k}_1 + \mathbf{k}_2, \mathbf{k} - \mathbf{k}_1 - \mathbf{k}_2) f(|\mathbf{k}_1 + \mathbf{k}_2|) \\ & \times |\mathbf{k}_1 + \mathbf{k}_2| v_{\mathbf{k}_1 + \mathbf{k}_2}(\mathbf{k}_1, \mathbf{k}_2) f(|\mathbf{k} - \mathbf{k}_1 - \mathbf{k}_2|) S(|\mathbf{k} - \mathbf{k}_1 - \mathbf{k}_2|) f(k_2) S(k_2) \\ & \times v_{\mathbf{k} - \mathbf{k}_1}(\mathbf{k} - \mathbf{k}_1 - \mathbf{k}_2, \mathbf{k}_2) |\mathbf{k} - \mathbf{k}_1| f(|\mathbf{k} - \mathbf{k}_1|) f(k_1) S(k_1) v_{\mathbf{k}}(\mathbf{k}_1, \mathbf{k} - \mathbf{k}_1) + o(t^2) \end{aligned} \quad (39)$$

As mentioned above, the origin of the leading term Eq. (39) is the fact that integrations over intermediate times are unrestricted.

The problem described above forces us to be a little more careful while calculating corrections to the irreducible memory function. In the next two subsections we consider corrections

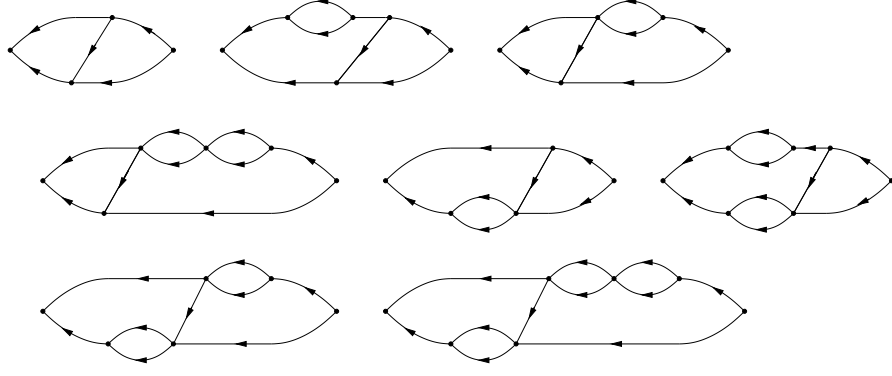


Fig. 8 Example diagrams that separate into two disconnected pieces upon removing the left and right vertices and cutting through a single propagator line. These diagrams have an additional property: if the response function-like insertion which makes the diagram a non-mode-coupling diagram is removed together with its beginning and ending vertices, there is no continuous path from the the right vertex to the left vertex.

originating from two classes of non-mode-coupling diagrams. The first class includes, among others, diagrams that can be obtained from the 2nd diagram at the right-hand-side of the diagrammatic equation in Fig. 5 by replacing the bare response functions G_0 by diagrams that appear in the diagrammatic expansion for the full response function. The second class includes, among others, diagrams that can be obtained from the 3rd diagram at the right-hand-side of Fig. 5 by replacing the bare response functions G_0 by diagrams that appear in the diagrammatic expansion for the full response function. We show that by re-summing each of the two classes of diagrams we get well-behaving corrections to the irreducible memory function.

4.2. The first correction

If one propagator line is cut in the 2nd diagram in the expansion showed in Fig. 5, this diagram turns into the 1st diagram in this expansion, *i.e* into a mode-coupling diagram. As the first correction we will re-sum the following well defined class of diagrams: all diagrams that turn into mode-coupling diagrams contributing to the irreducible memory function upon removing one response function-like insertion. In other words, these are the diagrams that contribute to the irreducible memory function and separate into two disconnected pieces upon removing the left and right vertices and cutting through a single propagator line. In addition, we will impose the following additional condition: if the response function-like insertion that makes the diagram a non-mode-coupling diagram is removed together with its beginning and ending vertices, there should be no continuous path from the the right vertex to the left vertex.

In Fig. 8 we show a few representative diagrams that are to be re-summed. While performing the re-summation one has to remember that the diagrams with odd and even number of four-leg vertices contribute with negative and positive sign, respectively. In Fig. 9 we show an example of a diagram which separates into two disconnected pieces upon removing the left and right vertices and cutting through a single propagator line but which does not have the additional property described above. Diagrams similar to that in Fig. 9 are not included in the

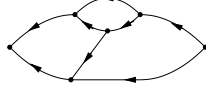


Fig. 9 An example diagram that turns into a mode-coupling diagram upon removing the left and right vertices and cutting through a single propagator line. For this diagram, if the response function-like insertion which makes the diagram a non-mode-coupling diagram is removed together with its beginning and ending vertices, there is still continuous path from the the right vertex to the left vertex.

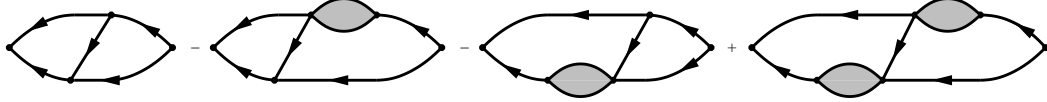


Fig. 10 The result of the re-summation of diagrams that separate into two disconnected pieces upon removing the left and right vertices and cutting through a single propagator line. The re-summed diagrams have an additional property: if the response function-like insertion which makes the diagram a non-mode-coupling diagram is removed together with its beginning and ending vertices, there is no continuous path from the the right vertex to the left vertex.

re-summation proposed here. The main reason for this additional requirement is the simplicity of the resulting expressions. Including all non-mode-coupling diagrams that turn into mode-coupling diagrams upon removing one response function-like insertion (*e.g.* including diagram showed in Fig. 9 and similar diagrams) is more complicated and will be discussed elsewhere [41].

The result of the re-summation of the above described class of diagrams is showed in Fig. 10 (bubble insertions in this figure are the memory function matrices defined in Eq. (26) and illustrated in Fig. 3). Briefly, the first two diagrams showed in Fig. 8 contribute to the first diagram in Fig. 10. This diagram is identical to the diagram showed in Fig. 7. The third and fourth diagrams in Fig. 8 contribute to the second diagram in Fig. 10. The fifth and sixth diagrams in Fig. 8 contribute to the third diagram in Fig. 10. Finally, the seventh and eighth diagrams in Fig. 8 contribute to the fourth diagram in Fig. 10.

The four diagrams showed in Fig. 10 lead to the following contribution to the irreducible memory function:

$$\begin{aligned}
\delta M_1^{\text{irr}}(k; t) = & n^2 D_0^3 \int_0^t dt_4 \int_0^{t_4} dt_3 \int_0^{t_3} dt_2 \int_0^{t_2} dt_1 \int \frac{d\mathbf{k}_1 d\mathbf{k}_2}{(2\pi)^6} v_{\mathbf{k}}(\mathbf{k}_1 + \mathbf{k}_2, \mathbf{k} - \mathbf{k}_1 - \mathbf{k}_2) \\
& \times G(|\mathbf{k}_1 + \mathbf{k}_2|; t - t_4) (\delta(t_4 - t_3) - M(|\mathbf{k}_1 + \mathbf{k}_2|; t_4 - t_3)) |\mathbf{k}_1 + \mathbf{k}_2| v_{\mathbf{k}_1 + \mathbf{k}_2}(\mathbf{k}_1, \mathbf{k}_2) \\
& \times G(|\mathbf{k} - \mathbf{k}_1 - \mathbf{k}_2|; t - t_1) S(|\mathbf{k} - \mathbf{k}_1 - \mathbf{k}_2|) G(k_2; t_3 - t_2) S(k_2) \\
& \times v_{\mathbf{k} - \mathbf{k}_1}(\mathbf{k} - \mathbf{k}_1 - \mathbf{k}_2, \mathbf{k}_2) |\mathbf{k} - \mathbf{k}_1| (\delta(t_2 - t_1) - M(|\mathbf{k} - \mathbf{k}_1|; t_2 - t_1)) G(|\mathbf{k} - \mathbf{k}_1|; t_1) \\
& \times G(k_1; t_3) S(k_1) v_{\mathbf{k}}(\mathbf{k}_1, \mathbf{k} - \mathbf{k}_1).
\end{aligned} \tag{40}$$

To show that these four diagrams give a well-behaving contribution we will first rewrite Eq. (40). To this end we will use the following two identities which can be obtained from Eq.

(22),

$$\begin{aligned} & \int_0^t dt_1 (\delta(t - t_1) - M(k; t - t_1)) G(k; t_1) \\ &= \int_0^t dt_1 G(k; t - t_1) (\delta(t_1) - M(k; t_1)) = -\frac{S(k)}{D_0 k^2} \partial_t G(k; t). \end{aligned} \quad (41)$$

These identities allow us to rewrite Eq. (40) in the following form

$$\begin{aligned} \delta M_1^{\text{irr}}(k; t) &= n^2 D_0 \int_0^t dt_3 \int_0^{t_3} dt_2 \int \frac{d\mathbf{k}_1 d\mathbf{k}_2}{(2\pi)^6} v_{\mathbf{k}}(\mathbf{k}_1 + \mathbf{k}_2, \mathbf{k} - \mathbf{k}_1 - \mathbf{k}_2) \\ &\times \partial_t G(|\mathbf{k}_1 + \mathbf{k}_2|; t - t_3) S(|\mathbf{k}_1 + \mathbf{k}_2|) \tilde{v}_{\mathbf{k}_1 + \mathbf{k}_2}(\mathbf{k}_1, \mathbf{k}_2) G(|\mathbf{k} - \mathbf{k}_1 - \mathbf{k}_2|; t - t_1) \\ &\times S(|\mathbf{k} - \mathbf{k}_1 - \mathbf{k}_2|) G(k_2; t_3 - t_2) S(k_2) \tilde{v}_{\mathbf{k} - \mathbf{k}_1}(\mathbf{k} - \mathbf{k}_1 - \mathbf{k}_2, \mathbf{k}_2) \\ &\times \partial_{t_2} G(|\mathbf{k} - \mathbf{k}_1|; t_2) S(|\mathbf{k} - \mathbf{k}_1|) G(k_1; t_3) S(k_1) v_{\mathbf{k}}(\mathbf{k}_1, \mathbf{k} - \mathbf{k}_1), \end{aligned} \quad (42)$$

where modified vertex function \tilde{v} is defined in Eq. (13).

Now we can appreciate the effect of adding to the first diagram in Fig. 10 (which is identical to the diagram showed in Fig. 7 and discussed in the previous subsection) the remaining three diagrams. Roughly speaking, by adding the additional diagrams two response functions in the first diagram in Fig. 10 get replaced by time derivatives of response functions. As a result, restrictions for integrations over intermediate times are introduced. To see this we need to recognize the fact that even if the full response function develops a long-lived plateau, its time derivative still decays fast. In particular, if the full response function acquires a non-vanishing long-time limit, its time derivative can be trivially integrated over time. Thus, if $\lim_{t \rightarrow \infty} G(k; t) = f(k)$, then the long-time limit of correction (42) is finite and given by the following expression:

$$\begin{aligned} \lim_{t \rightarrow \infty} \delta M_1^{\text{irr}}(k; t) &= n^2 D_0 \int_0^t dt_3 \int_0^{t_3} dt_2 \int \frac{d\mathbf{k}_1 d\mathbf{k}_2}{(2\pi)^6} v_{\mathbf{k}}(\mathbf{k}_1 + \mathbf{k}_2, \mathbf{k} - \mathbf{k}_1 - \mathbf{k}_2) \\ &\times (1 - f(|\mathbf{k}_1 + \mathbf{k}_2|)) S(|\mathbf{k}_1 + \mathbf{k}_2|) \tilde{v}_{\mathbf{k}_1 + \mathbf{k}_2}(\mathbf{k}_1, \mathbf{k}_2) f(|\mathbf{k} - \mathbf{k}_1 - \mathbf{k}_2|) \\ &\times S(|\mathbf{k} - \mathbf{k}_1 - \mathbf{k}_2|) f(k_2) S(k_2) \tilde{v}_{\mathbf{k} - \mathbf{k}_1}(\mathbf{k} - \mathbf{k}_1 - \mathbf{k}_2, \mathbf{k}_2) \\ &\times (1 - f(|\mathbf{k} - \mathbf{k}_1|)) S(|\mathbf{k} - \mathbf{k}_1|) f(k_1) S(k_1) v_{\mathbf{k}}(\mathbf{k}_1, \mathbf{k} - \mathbf{k}_1). \end{aligned} \quad (43)$$

It is instructive to derive from the above expression the contribution to the function m defined in Eq. (36):

$$\begin{aligned} \delta m_1(k) &= \lim_{t \rightarrow \infty} \frac{S(k)}{D_0 k^2} \delta M_1^{\text{irr}}(k; t) = n^2 S(k) \int \frac{d\mathbf{k}_1 d\mathbf{k}_2}{(2\pi)^6} \tilde{v}_{\mathbf{k}}(\mathbf{k}_1 + \mathbf{k}_2, \mathbf{k} - \mathbf{k}_1 - \mathbf{k}_2) \\ &\times (1 - f(|\mathbf{k}_1 + \mathbf{k}_2|)) S(|\mathbf{k}_1 + \mathbf{k}_2|) \tilde{v}_{\mathbf{k}_1 + \mathbf{k}_2}(\mathbf{k}_1, \mathbf{k}_2) f(|\mathbf{k} - \mathbf{k}_1 - \mathbf{k}_2|) \\ &\times S(|\mathbf{k} - \mathbf{k}_1 - \mathbf{k}_2|) f(k_2) S(k_2) \tilde{v}_{\mathbf{k} - \mathbf{k}_1}(\mathbf{k} - \mathbf{k}_1 - \mathbf{k}_2, \mathbf{k}_2) \\ &\times (1 - f(|\mathbf{k} - \mathbf{k}_1|)) S(|\mathbf{k} - \mathbf{k}_1|) f(k_1) S(k_1) \tilde{v}_{\mathbf{k}}(\mathbf{k}_1, \mathbf{k} - \mathbf{k}_1). \end{aligned} \quad (44)$$

It can be seen that the above expression can be interpreted as a renormalized diagram. The vertices of this diagram are given by the modified vertex functions $\tilde{v}_{\mathbf{k}}$ and the bonds are equal to either $f(k)S(k)$ or $(1 - f(k))S(k)$. Alternatively, using relation (35) between $f(k)$ and $m(k)$, the above expression can be re-written in such a way that the internal vertices of the renormalized diagram are given by $\tilde{v}_{\mathbf{k}}/m(k)$ and all the bonds are equal to $f(k)S(k)$. We

will see in the next section that the expression for the second correction can be written in a similar way.

A priori, it is not clear whether the above expression is positive or negative, *i.e.* whether it moves the ergodicity breaking transition of the standard mode-coupling theory towards higher or lower temperatures (or lower or higher volume fractions), respectively. The explicit calculation described in subsection 4.4 suggests that expression (43) gives a small, positive contribution to the irreducible memory function.

4.3. The second correction

If one propagator line is cut in the 3rd diagram in the expansion showed in Fig. 5, this diagram turns into one of the mode-coupling diagrams contributing to the *reducible* memory matrix. Specifically, by removing one propagator line we can turn the 3rd diagram in the expansion in Fig. 5 into the second diagram in the expansion in Fig. 3. As the second correction we will re-sum the following class of diagrams: all diagrams that turn into mode-coupling diagrams contributing to the memory matrix upon removing one response function-like insertion. In addition, we will impose an additional condition which is similar to that introduced in Sec. 4.2. In the present case the description of this additional condition is a little more complicated, but the idea is the same. We will re-sum only those diagrams for which, if the response function-like insertion which makes the diagram a non-mode-coupling diagram is removed together with its beginning and ending vertices, there is only one continuous path from the right vertex to the closest articulation four-leg vertex and only one continuous path from the left vertex to the closest articulation four-leg vertex.

In Fig. 11 we show a few representative diagrams that are to be re-summed. Again, while performing the re-summation one has to remember that the diagrams with odd and even number of four-leg vertices contribute with negative and positive sign, respectively. In Fig. 12 we show an example of a diagram which does not have the additional property described in the preceding paragraph. In the diagram showed in Fig. 12, if the response function-like insertion together with its beginning and ending vertices is removed, there are two continuous paths from the right vertex to the closest articulation four-leg vertex (which is the only four-leg vertex in this diagram) and two continuous paths from the left vertex to the closest articulation four-leg vertex. Diagrams similar to that in Fig. 12 are not included in the re-summation proposed here. Again, the main reason for this additional requirement is the simplicity of the resulting expressions.

The result of the re-summation of the above described class of diagrams is showed in Fig. 13. Again, unlabeled bubble insertions are the memory function matrices defined in Eq. (26) and illustrated in Fig. 3. In contrast, bubble insertions labeled MCT are the memory function matrices within the mode-coupling approximation showed in Fig. 14. The presence of the latter insertions are the consequence of the definition of the class of diagrams that are re-summed in this subsection. Specifically, we imposed the requirement that after one response function-like insertion is removed, the resulting diagram was a mode-coupling diagram contributing to the memory matrix. The last condition means that after the response function-like insertion is removed (but its beginning and ending vertices are kept) the resulting diagram has to have the following property: if the left and right vertices, and the four-leg articulation vertices are

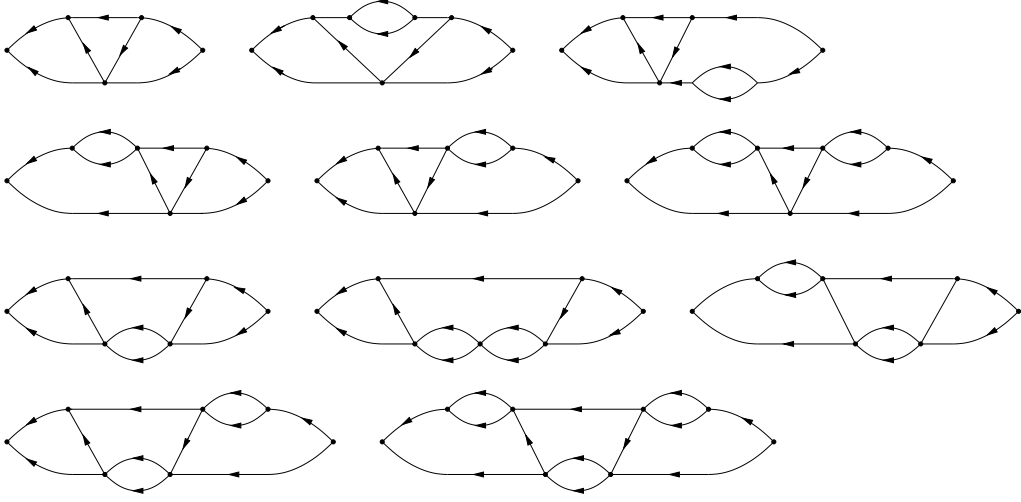


Fig. 11 Example diagrams that turn into mode-coupling contributions to the memory matrix upon removing one response function-like insertion. These diagrams have an additional property: if the response function-like insertion which makes the diagram a non-mode-coupling diagram is removed together with its beginning and ending vertices, there is only one continuous path from the right vertex to the closest articulation four-leg vertex and only one continuous path from the left vertex to the closest articulation four-leg vertex.

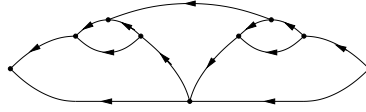


Fig. 12 An example diagram that turns into mode-coupling-like contributions to the memory matrix upon removing one response function-like insertion. For this diagram, if the response function-like insertion which makes the diagram a non-mode-coupling diagram is removed together with its beginning and ending vertices, there are two continuous paths from the right vertex to the closest articulation four-leg vertex (which is the only four-leg vertex in this diagram) and two continuous paths from the left vertex to the closest articulation four-leg vertex.

removed from the diagram, each part that used to be between successive articulation vertices has to consist of two disconnected pieces.

Briefly, the first three diagrams showed in Fig. 11 contribute to the first diagram in Fig. 13. The fourth, fifth and sixth diagrams in Fig. 11 contribute to the second, third, and fourth diagrams in Fig. 13, respectively. The seventh and eighth diagrams in Fig. 11 contribute to the fifth diagram in Fig. 13. Finally, the ninth, tenth and eleventh diagrams in Fig. 11 contribute to the sixth, seventh, and eighth diagrams in Fig. 13, respectively.

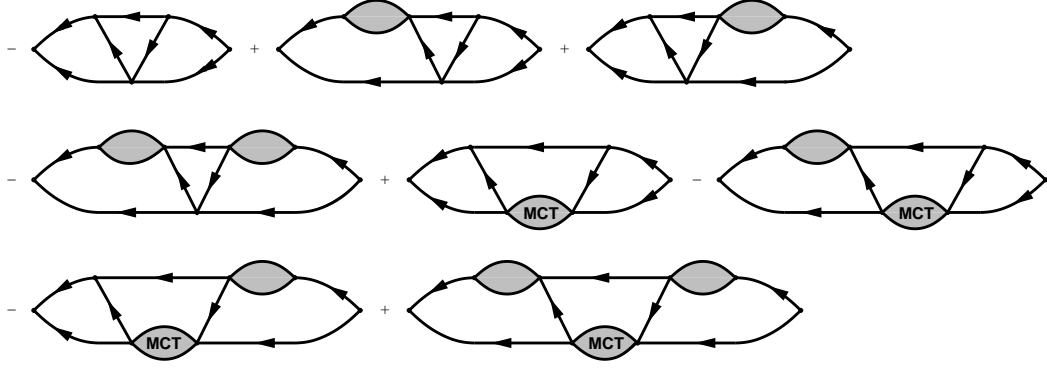


Fig. 13 The result of the re-summation of diagrams that turn into mode-coupling-like contributions to the memory function upon removing one response function-like insertion. The re-summed diagrams have an additional property: if the response function-like insertion together with its beginning and ending vertices is removed, there is only one continuous path from the right vertex to the closest articulation four-leg vertex and only one continuous path from the left vertex to the closest articulation four-leg vertex.

Fig. 14 Memory matrix \mathbf{M} calculated within the mode-coupling approximation.

The eight diagrams showed in Fig. 13 lead to the following contribution to the irreducible memory function:

$$\begin{aligned}
\delta M_2^{\text{irr}}(k; t) = & -n^3 D_0^4 \int_0^t dt_6 \int_0^{t_6} dt_5 \int_0^{t_5} dt_4 \int_0^{t_4} dt_3 \int_0^{t_3} dt_2 \int_0^{t_2} dt_1 \int \frac{d\mathbf{k}_1 d\mathbf{k}_2 d\mathbf{k}_3}{(2\pi)^9} \\
& \times v_{\mathbf{k}}(\mathbf{k}_1 + \mathbf{k}_2 - \mathbf{k}_3, \mathbf{k} - \mathbf{k}_1 - \mathbf{k}_2 + \mathbf{k}_3) G(|\mathbf{k}_1 + \mathbf{k}_2 - \mathbf{k}_3|; t - t_4) S(|\mathbf{k}_1 + \mathbf{k}_2 - \mathbf{k}_3|) \\
& \times G(|\mathbf{k} - \mathbf{k}_1 - \mathbf{k}_2 + \mathbf{k}_3|; t - t_6) (\delta(t_6 - t_5) - M(|\mathbf{k} - \mathbf{k}_1 - \mathbf{k}_2 + \mathbf{k}_3|; t_6 - t_5)) \\
& |\mathbf{k} - \mathbf{k}_1 - \mathbf{k}_2 + \mathbf{k}_3| v_{\mathbf{k}-\mathbf{k}_1-\mathbf{k}_2+\mathbf{k}_3}(\mathbf{k} - \mathbf{k}_1 - \mathbf{k}_2, \mathbf{k}_3) G(k_3; t_5 - t_4) S(k_3) \\
& G(|\mathbf{k} - \mathbf{k}_1 - \mathbf{k}_2|; t_5 - t_2) S(|\mathbf{k} - \mathbf{k}_1 - \mathbf{k}_2|) \\
& \mathbf{v}(\mathbf{k}_1 + \mathbf{k}_2 - \mathbf{k}_3, \mathbf{k}_3) \cdot [\mathcal{I} \delta(t_4 - t_3) - \mathbf{M}_{\text{MCT}}(\mathbf{k}_1 + \mathbf{k}_2; t_4 - t_3)] \cdot \mathbf{v}(\mathbf{k}_1, \mathbf{k}_2) \\
& G(k_2; t_3 - t_2) S(k_2) v_{\mathbf{k}-\mathbf{k}_1}(\mathbf{k}_2, \mathbf{k} - \mathbf{k}_1 - \mathbf{k}_2) |\mathbf{k} - \mathbf{k}_1| \\
& (\delta(t_2 - t_1) - M(|\mathbf{k} - \mathbf{k}_1|; t_2 - t_1)) G(|\mathbf{k} - \mathbf{k}_1|; t_1) G(k_1; t_3) S(k_1) v_{\mathbf{k}}(\mathbf{k}_1, \mathbf{k} - \mathbf{k}_1),
\end{aligned} \tag{45}$$

where \mathcal{I} denotes the unit tensor. To write down Eq. (45) in a slightly more compact form we used the function \mathbf{v} defined in Eq. (12) and we introduced the mode-coupling theory's memory matrix that has the delta function originating from translational invariance factored out,

$$\mathbf{M}_{\text{MCT}}(\mathbf{k}, \mathbf{k}_1; t) = \mathbf{M}_{\text{MCT}}(\mathbf{k}; t) (2\pi)^3 \delta(\mathbf{k} - \mathbf{k}_1), \tag{46}$$

where $\mathbf{M}_{\text{MCT}}(\mathbf{k}, \mathbf{k}_1; t)$ is the memory matrix calculated within the mode-coupling approximation (see Fig. 14). For future use (see Eq. (49) below) we also define mode-coupling theory's

irreducible memory matrix with the delta function part factored out,

$$\mathbf{M}_{\text{MCT}}^{\text{irr}}(\mathbf{k}, \mathbf{k}_1; t) = \mathbf{M}_{\text{MCT}}^{\text{irr}}(\mathbf{k}; t)(2\pi)^3 \delta(\mathbf{k} - \mathbf{k}_1). \quad (47)$$

It should be noted that we use the same symbols for memory matrices with and without delta function factors. Whenever we use memory matrices with delta functions factored out, we will indicate this fact by specifying their arguments.

As in the previous subsection, we can use identities (41) to replace the memory functions (but not the mode-coupling memory matrix) by time derivatives,

$$\begin{aligned} \delta M_2^{\text{irr}}(k; t) = & -n^3 D_0^2 \int_0^5 dt_5 \int_0^{t_5} dt_4 \int_0^{t_4} dt_3 \int_0^{t_3} dt_2 \int \frac{d\mathbf{k}_1 d\mathbf{k}_2 d\mathbf{k}_3}{(2\pi)^9} \\ & \times v_{\mathbf{k}}(\mathbf{k}_1 + \mathbf{k}_2 - \mathbf{k}_3, \mathbf{k} - \mathbf{k}_1 - \mathbf{k}_2 + \mathbf{k}_3) G(|\mathbf{k}_1 + \mathbf{k}_2 - \mathbf{k}_3|; t - t_4) S(|\mathbf{k}_1 + \mathbf{k}_2 - \mathbf{k}_3|) \\ & \times \partial_t G(|\mathbf{k} - \mathbf{k}_1 - \mathbf{k}_2 + \mathbf{k}_3|; t - t_5) S(|\mathbf{k} - \mathbf{k}_1 - \mathbf{k}_2 + \mathbf{k}_3|) \\ & \times |\mathbf{k} - \mathbf{k}_1 - \mathbf{k}_2 + \mathbf{k}_3| \tilde{v}_{\mathbf{k} - \mathbf{k}_1 - \mathbf{k}_2 + \mathbf{k}_3}(\mathbf{k} - \mathbf{k}_1 - \mathbf{k}_2, \mathbf{k}_3) G(k_3; t_5 - t_4) S(k_3) \\ & \times G(|\mathbf{k} - \mathbf{k}_1 - \mathbf{k}_2|; t_5 - t_2) S(|\mathbf{k} - \mathbf{k}_1 - \mathbf{k}_2|) \\ & \times \mathbf{v}(\mathbf{k}_1 + \mathbf{k}_2 - \mathbf{k}_3, \mathbf{k}_3) \cdot [\mathcal{I} \delta(t_4 - t_3) - \mathbf{M}_{\text{MCT}}(\mathbf{k}_1 + \mathbf{k}_2; t_4 - t_3)] \cdot \mathbf{v}(\mathbf{k}_1, \mathbf{k}_2) \\ & \times G(k_2; t_3 - t_2) S(k_2) \tilde{v}_{\mathbf{k} - \mathbf{k}_1}(\mathbf{k}_2, \mathbf{k} - \mathbf{k}_1 - \mathbf{k}_2) \\ & \times \partial_{t_2} G(|\mathbf{k} - \mathbf{k}_1|; t_2) S(|\mathbf{k} - \mathbf{k}_1|) G(k_1; t_3) S(k_1) v_{\mathbf{k}}(\mathbf{k}_1, \mathbf{k} - \mathbf{k}_1), \end{aligned} \quad (48)$$

where the modified vertex function \tilde{v} is defined in Eq. (13).

Again, the above expression has a well defined, finite long-time limit, even if the full response function does not decay. To see this we need to recognize two facts. First, as before, the presence of time derivatives introduces restrictions for integrations over intermediate times. Second, the term $[\mathcal{I} \delta(t) - \mathbf{M}_{\text{MCT}}(\mathbf{k}; t)]$ introduces an additional restriction for integration over intermediate times. Technically, the last statement follows from the fact that if $\lim_{t \rightarrow \infty} G(k; t) = f(k)$, then the irreducible memory matrix does not decay, $\lim_{t \rightarrow \infty} \mathbf{M}_{\text{MCT}}^{\text{irr}}(\mathbf{k}; t) \neq 0$, and consequently the Laplace transform of this term vanishes as $z \rightarrow 0$,

$$\mathcal{I} - \mathbf{M}_{\text{MCT}}(\mathbf{k}; z) = [\mathcal{I} + \mathbf{M}_{\text{MCT}}^{\text{irr}}(\mathbf{k}; z)]^{-1} \rightarrow z \left[\lim_{t \rightarrow \infty} \mathbf{M}_{\text{MCT}}^{\text{irr}}(\mathbf{k}; t) \right]^{-1} + o(z). \quad (49)$$

The presence of both restrictions on integrations over intermediate times makes the long-time limit of correction (48) well defined. We can show that if $\lim_{t \rightarrow \infty} G(k; t) = f(k)$ then

the long-time limit of correction (48) is given by the following expression:

$$\begin{aligned}
\delta M_2^{\text{irr}}(k; t) = & -n^3 D_0 \int \frac{d\mathbf{k}_1 d\mathbf{k}_2 d\mathbf{k}_3}{(2\pi)^9} \\
& \times v_{\mathbf{k}}(\mathbf{k}_1 + \mathbf{k}_2 - \mathbf{k}_3, \mathbf{k} - \mathbf{k}_1 - \mathbf{k}_2 + \mathbf{k}_3) f(|\mathbf{k}_1 + \mathbf{k}_2 - \mathbf{k}_3|) S(|\mathbf{k}_1 + \mathbf{k}_2 - \mathbf{k}_3|) \\
& \times (1 - f(|\mathbf{k} - \mathbf{k}_1 - \mathbf{k}_2 + \mathbf{k}_3|)) S(|\mathbf{k} - \mathbf{k}_1 - \mathbf{k}_2 + \mathbf{k}_3|) \\
& \times |\mathbf{k} - \mathbf{k}_1 - \mathbf{k}_2 + \mathbf{k}_3| \tilde{v}_{\mathbf{k}-\mathbf{k}_1-\mathbf{k}_2+\mathbf{k}_3}(\mathbf{k} - \mathbf{k}_1 - \mathbf{k}_2, \mathbf{k}_3) f(k_3) S(k_3) \\
& \times f(|\mathbf{k} - \mathbf{k}_1 - \mathbf{k}_2|) S(|\mathbf{k} - \mathbf{k}_1 - \mathbf{k}_2|) S(|\mathbf{k}_1 + \mathbf{k}_2|) \\
& \times [\tilde{v}_{\mathbf{k}_1+\mathbf{k}_2}(\mathbf{k}_1 + \mathbf{k}_2 - \mathbf{k}_3, \mathbf{k}_3) \tilde{v}_{\mathbf{k}_1+\mathbf{k}_2}(\mathbf{k}_1, \mathbf{k}_2) m_{\text{MCT}}^{-1}(|\mathbf{k}_1 + \mathbf{k}_2|) \\
& + (\tilde{\mathbf{v}}(\mathbf{k}_1 + \mathbf{k}_2 - \mathbf{k}_3, \mathbf{k}_3) \cdot \tilde{\mathbf{v}}(\mathbf{k}_1, \mathbf{k}_2) - \tilde{v}_{\mathbf{k}_1+\mathbf{k}_2}(\mathbf{k}_1 + \mathbf{k}_2 - \mathbf{k}_3, \mathbf{k}_3) \tilde{v}_{\mathbf{k}_1+\mathbf{k}_2}(\mathbf{k}_1, \mathbf{k}_2)) \\
& \times m_{\text{tMCT}}^{-1}(|\mathbf{k}_1 + \mathbf{k}_2|)] f(k_2) S(k_2) \tilde{v}_{\mathbf{k}-\mathbf{k}_1}(\mathbf{k}_2, \mathbf{k} - \mathbf{k}_1 - \mathbf{k}_2) \\
& \times (1 - f(|\mathbf{k} - \mathbf{k}_1|)) S(|\mathbf{k} - \mathbf{k}_1|) f(k_1) S(k_1) v_{\mathbf{k}}(\mathbf{k}_1, \mathbf{k} - \mathbf{k}_1). \tag{50}
\end{aligned}$$

Again, to write Eq. (50) in a slightly more compact form we used modified vertex functions \tilde{v} and $\tilde{\mathbf{v}}$ defined in Eqs. (13-14) and function m_{MCT} defined in Eq. (37). Furthermore, the function m_{tMCT} in Eq. (50) is related to the transverse part of the mode-coupling theory's irreducible memory matrix through the following equations,

$$(\mathcal{I} - \hat{\mathbf{k}}\hat{\mathbf{k}}) : \mathbf{M}_{\text{MCT}}^{\text{irr}}(\mathbf{k}, \mathbf{k}_1; t) = 2M_{\text{tMCT}}(k; t) (2\pi)^3 \delta(\mathbf{k} - \mathbf{k}_1), \tag{51}$$

$$m_{\text{tMCT}}(k) = \lim_{t \rightarrow \infty} \frac{S(k)}{D_0 k^2} M_{\text{tMCT}}(k; t). \tag{52}$$

We shall point out that, to the best of our knowledge, the transverse part of the irreducible memory function has never appeared before in any theory of the dynamics of Brownian systems. It is not entirely clear whether its appearance in Eq. (50) is a result of one of approximations involved in deriving this equation or whether it has a more fundamental origin.

As in the previous subsection, it is instructive to derive from the above expression the contribution to the function m defined in Eq. (36):

$$\begin{aligned}
\delta m_2(k) = & \lim_{t \rightarrow \infty} \frac{S(k)}{D_0 k^2} \delta M_2^{\text{irr}}(k; t) = -n^3 S(k) \int \frac{d\mathbf{k}_1 d\mathbf{k}_2 d\mathbf{k}_3}{(2\pi)^9} \\
& \times \tilde{v}_{\mathbf{k}}(\mathbf{k}_1 + \mathbf{k}_2 - \mathbf{k}_3, \mathbf{k} - \mathbf{k}_1 - \mathbf{k}_2 + \mathbf{k}_3) f(|\mathbf{k}_1 + \mathbf{k}_2 - \mathbf{k}_3|) S(|\mathbf{k}_1 + \mathbf{k}_2 - \mathbf{k}_3|) \\
& \times (1 - f(|\mathbf{k} - \mathbf{k}_1 - \mathbf{k}_2 + \mathbf{k}_3|)) S(|\mathbf{k} - \mathbf{k}_1 - \mathbf{k}_2 + \mathbf{k}_3|) \\
& \times |\mathbf{k} - \mathbf{k}_1 - \mathbf{k}_2 + \mathbf{k}_3| \tilde{v}_{\mathbf{k}-\mathbf{k}_1-\mathbf{k}_2+\mathbf{k}_3}(\mathbf{k} - \mathbf{k}_1 - \mathbf{k}_2, \mathbf{k}_3) f(k_3) S(k_3) \\
& \times f(|\mathbf{k} - \mathbf{k}_1 - \mathbf{k}_2|) S(|\mathbf{k} - \mathbf{k}_1 - \mathbf{k}_2|) S(|\mathbf{k}_1 + \mathbf{k}_2|) \\
& \times [\tilde{v}_{\mathbf{k}_1+\mathbf{k}_2}(\mathbf{k}_1 + \mathbf{k}_2 - \mathbf{k}_3, \mathbf{k}_3) \tilde{v}_{\mathbf{k}_1+\mathbf{k}_2}(\mathbf{k}_1, \mathbf{k}_2) m_{\text{MCT}}^{-1}(|\mathbf{k}_1 + \mathbf{k}_2|) \\
& + (\tilde{\mathbf{v}}(\mathbf{k}_1 + \mathbf{k}_2 - \mathbf{k}_3, \mathbf{k}_3) \cdot \tilde{\mathbf{v}}(\mathbf{k}_1, \mathbf{k}_2) - \tilde{v}_{\mathbf{k}_1+\mathbf{k}_2}(\mathbf{k}_1 + \mathbf{k}_2 - \mathbf{k}_3, \mathbf{k}_3) \tilde{v}_{\mathbf{k}_1+\mathbf{k}_2}(\mathbf{k}_1, \mathbf{k}_2)) \\
& \times m_{\text{tMCT}}^{-1}(|\mathbf{k}_1 + \mathbf{k}_2|)] f(k_2) S(k_2) \tilde{v}_{\mathbf{k}-\mathbf{k}_1}(\mathbf{k}_2, \mathbf{k} - \mathbf{k}_1 - \mathbf{k}_2) \\
& \times (1 - f(|\mathbf{k} - \mathbf{k}_1|)) S(|\mathbf{k} - \mathbf{k}_1|) f(k_1) S(k_1) \tilde{v}_{\mathbf{k}}(\mathbf{k}_1, \mathbf{k} - \mathbf{k}_1). \tag{53}
\end{aligned}$$

Furthermore, using relation (35) between f and m , we can re-write the above expression in such a way that it can be interpreted as a renormalized diagram. This diagram consists of

the left and right vertices given by $\tilde{v}_{\mathbf{k}}$, internal three-leg vertices given by $\tilde{v}_{\mathbf{k}}/m(k)$, a four-leg vertex that represents an expression involving $m_{\text{MCT}}(k)$ and $m_{\text{tMCT}}(k)$, and a bond equal to $f(k)S(k)$. We will comment on the possible significance of this form of the above expression in Sec. 5.

Again, *a priori*, it is not clear whether expression (53) is positive or negative. The explicit calculation described in the next subsection suggests that expression (50) gives a significant, negative contribution to the irreducible memory function.

4.4. Perturbative calculation of the two corrections

The two additional contributions to the irreducible memory function, Eqs. (42) and (48), are functionals of the full response function. In principle, these contributions can be added to the mode-coupling contribution, Eq. (33), and then the equation of motion for the response function,

$$\int_0^t dt_1 [\delta(t - t_1) + M_{\text{MCT}}^{\text{irr}}(k; t - t_1) + \delta M_1^{\text{irr}}(k; t - t_1) + \delta M_2^{\text{irr}}(k; t - t_1)] \partial_{t_1} G(k; t_1) = -\frac{D_0 k^2}{S(k)} G(t) \quad (54)$$

can be solved self-consistently. As the additional contributions are expressed in terms of many-dimensional integrals (over wave-vectors and time) of the full response function, this procedure seems difficult and will not be attempted here. A somewhat easier task would be to consider the self-consistent equation for the non-ergodicity parameter $f(k) = \lim_{t \rightarrow \infty} G(k; t)$,

$$\frac{f(k)}{1 - f(k)} = m_{\text{MCT}}(k) + \delta m_1(k) + \delta m_2(k), \quad (55)$$

where the functions at the right-hand-side are given by Eqs. (37), (44) and (53). This equation is a little more manageable because δm_1 and δm_2 are functionals of the non-ergodicity parameter only. However, the full self-consistent solution of Eq. (55) still seems rather difficult.

To get some feeling regarding the size of the two additional terms, δm_1 and δm_2 , contributing to the left-hand-side of Eq. (55) we will calculate them perturbatively. Specifically, we will first solve the standard mode-coupling equations for the non-ergodicity parameter, Eqs. (35) and (37). Then, we will use the resulting mode-coupling non-ergodicity parameter to calculate the additional contributions. These contributions will be then compared to the mode-coupling contribution m_{MCT} .

In order to perform numerical calculations we have to specify the system and its state, and an approximate theory that will be used to calculate the static structure factor for this system. As in our earlier work [30], we will use the hard sphere system at the ergodicity-breaking transition point of the standard mode-coupling theory and we will use the Verlet-Weiss approximation for the structure factor. We recall that using the Verlet-Weiss structure factor results in the ergodicity-breaking transition at volume fraction $\phi_{\text{MCT}} = 0.525$.

In Fig. 15 we compare the mode-coupling result for function m , m_{MCT} given by Eq. (37), with two corrections, δm_1 given by Eq. (44), and δm_2 given by Eq. (53). We can see that the first correction is rather small and, for most wave-vectors, positive. In contrast, the second correction is more significant, with its magnitude reaching above 20% of the mode-coupling

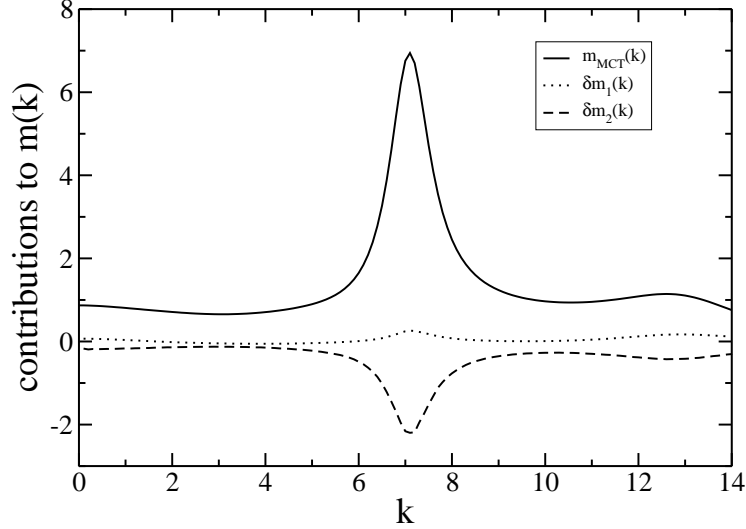


Fig. 15 Contributions to the $m(k) = \lim_{t \rightarrow \infty} (S(k)/D_0 k^2) M^{\text{irr}}(k; t)$, Eq. (36), calculated for a hard-sphere system using Verlet-Weiss structure factor at the mode-coupling transition, $\phi_{MCT} = 0.525$. Solid line: mode-coupling contribution, $m_{MCT}(k)$, Eq. (37). Dotted line: the first correction, $\delta m_1(k)$, Eq. (44). Dashed line: the second correction $\delta m_2(k)$, Eq. (53). The corrections are calculated perturbatively, *i.e.* using mode-coupling theory's non-ergodicity parameter $f(k)$.

contribution, and negative. Thus, the second correction dominates and it likely either moves the ergodicity breaking transition to higher volume fractions or removes it completely.

5. Discussion

We have showed here that our earlier diagrammatic approach to the dynamics of fluctuations in equilibrium systems of interacting Brownian particles can be used to derive corrections to mode-coupling theory's irreducible memory function. We have presented explicit expressions for the two simplest corrections and we have evaluated these corrections perturbatively. We found that one of these corrections, which in our perturbative calculation gives a negative contribution to the irreducible memory function, is comparable to the mode-coupling contribution. Thus, our results suggest that the simplest corrections are likely to move the ergodicity breaking transition to lower temperatures or higher volume fractions.

One important conclusion from our explicit calculations is that the easiest way to extend the standard mode-coupling theory is to concentrate on the self-consistent equation for the non-ergodicity parameter. This allows one to avoid complications associated with the time dependence and reduces the technical complexity of the equations that need to be solved.

Of course, while deriving approximate expressions for non-mode-coupling contributions to the irreducible memory function one should strive to work with diagrams with bonds representing the full response function. The second important conclusion from our calculations is that in order to avoid spurious, unphysical divergences one has to re-sum the original diagrammatic expansion in such a way that restrictions on intermediate time integrations are introduced.

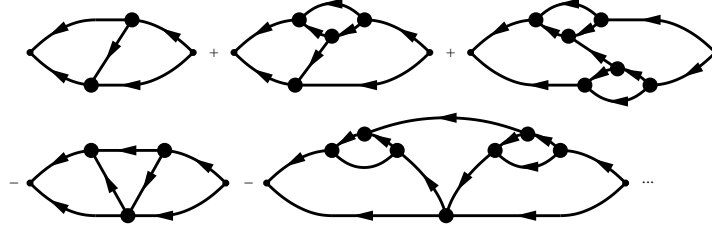


Fig. 16 Re-summation of one particle irreducible, non-mode-coupling, fully renormalized diagrams with the following property: if one line is cut, the diagram either becomes a mode-coupling diagram or a product of two mode-coupling diagrams.

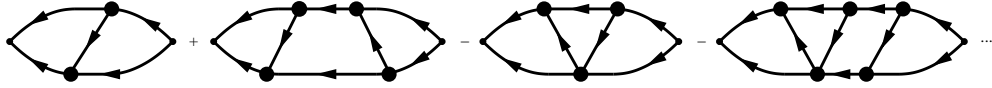


Fig. 17 Re-summation of one particle irreducible, non-mode-coupling, fully renormalized ladder diagrams where rungs of the ladders are non-mode-coupling parts of the two contributions discussed in the present paper.

Our final expressions suggest that it should be possible to derive a fully renormalized diagrammatic series expansion for function $m(k)$ that is related to the long-time limit of the irreducible memory function, Eq. (36). In diagrams contributing to $m(k)$ the left and right vertices are given by modified vertex function $\tilde{v}_{\mathbf{k}}$, Eq. (13). The bonds represent the long-time limit of the full intermediate scattering function, $\lim_{t \rightarrow \infty} F(k; t) \equiv f(k)S(k)$. The internal three-leg vertices represent modified vertex function $\tilde{v}_{\mathbf{k}}$ divided by $m(k)$. Finally, the internal four-leg vertices represent a combination of a product of two functions $\tilde{v}_{\mathbf{k}}$ divided by $m(k)$ and a novel term involving the transverse part of the memory matrix, $m_t(k)$. The internal three-leg vertices pick up factors involving $m(k)$ and the internal four-leg vertices pick up factors involving $m(k)$, and $m_t(k)$ as a result of re-summations that introduce restrictions on intermediate time integrations and thus remove spurious divergences. The fully renormalized diagrams which represent expressions (44) and (53) are the first and fourth diagrams in Fig. 16 or the first and third diagrams in Fig. 17.

In Fig. 16 we show one possible extension of the work presented here. In Secs. 4.2 and 4.3 we defined diagrams that were to be re-summed as, roughly speaking, mode-coupling diagrams with one extra response function-like insertions and with additional conditions. Here we remove these additional conditions. As a result, in addition to the first and fourth diagrams in Fig. 16, we get a whole class of fully renormalized diagrams, some of which are showed in Fig. 16. Preliminary results [41] suggest that if these diagrams are re-summed perturbatively (*i.e.* if mode-coupling f , m and m_t are used instead of the exact functions), the sum of these diagrams diverges upon approaching the ergodicity breaking transition of the standard mode-coupling theory. The strength of the divergence depends on the dimensionality of the system and the divergence vanishes in high enough dimension. The analysis of this divergence should allow us to calculate the upper critical dimension of the mode-coupling theory. An analogous calculation in the framework of the static replica approach appeared recently [42].

In Fig. 17 we show the second possible extension. Roughly speaking, we propose to re-sum a series of fully renormalized ladder diagrams where rungs of the ladders are represented by non-mode-coupling parts of the two contributions discussed in this paper (which are represented by the first and third diagrams in Fig. 17). This re-summation could be combined with Eq. (35) resulting in a self-consistent calculation.

Finally, we could also attempt to use the fully renormalized diagrammatic series to derive a self-consistent equation for a vertex function.

Acknowledgments

Part of this work was done when I was a Visiting Professor at Yukawa Institute for Theoretical Physics in Kyoto. I would like to acknowledge the Institute for its generous hospitality. I am grateful to Hisao Hayakawa for many insightful discussions during my stay in Kyoto and for the invitation to write this paper. I thank Elijah Flenner, Matthias Fuchs, Hisao Hayakawa and Koshiro Suzuki for their comments on the manuscript. Support by NSF Grant CHE 0909676 is gratefully acknowledged.

References

- [1] E. Leutheusser, Phys. Rev. A **29**, 2765, (1984).
- [2] U. Bengtzelius, W. Götze and A. Sjölander, J. Phys. C **17**, 5915, (1984).
- [3] S.P. Das, G.F. Mazenko, S. Ramaswamy and J.J. Toner, Phys. Rev. Lett. **54**, 118 (1985).
- [4] See, *e.g.*, a review by W. Kob, 2003, in *Slow Relaxations and Nonequilibrium Dynamics in Condensed Matter*, J.-L. Barrat, M. V. Feigelman, J. Kurchan, and J. Dalibard, eds. (Springer-Verlag, Berlin).
- [5] See, *e.g.*, a review by W. Götze, J. Phys.: Condens. Matter **11**, A1, (1999).
- [6] W. Götze, *Complex dynamics of glass-forming liquids: A mode-coupling theory* (Oxford University Press, Oxford, 2008).
- [7] M. Nauroth and W. Kob, Phys. Rev. E **55**, 657 (1997).
- [8] W. Kob, M. Nauroth and F. Sciortino, J. Non-Cryst. Solids, **307-310**, 181 (2002).
- [9] T. Gleim and W. Kob, Eur. Phys. J. B **13**, 83 (2000).
- [10] F. Weysser, A.M. Puertas, M. Fuchs and Th. Voigtmann, Phys. Rev. E **82**, 011504 (2010).
- [11] For a recent review of experimental, simulational, and theoretical studies of dynamic heterogeneities see *Dynamical Heterogeneities in Glasses, Colloids, and Granular Media*, L. Berthier, , G. Biroli, J.-P. Bouchaud, L. Cipelletti, and W. van Saarloos, eds. (Oxford University Press, Oxford, 2011).
- [12] G. Biroli, J.-P. Bouchaud, K. Miyazaki, and D. R. Reichman, Phys. Rev. Lett. **97**, 195701 (2006).
- [13] B. Schmid and R. Schilling, Phys. Rev. E **81**, 041502 (2010).
- [14] A. Ikeda and K. Miyazaki, Phys. Rev. Lett. **106**, 015701 (2011).
- [15] M. Mézard and G. Parisi, Phys. Rev. Lett. **82**, 747 (1999); J. Chem. Phys. **111**, 1076 (1999).
- [16] G. Parisi and F. Zamponi, Rev. Mod. Phys. **82**, 789 (2010).
- [17] P. Charbonneau , A. Ikeda, G. Parisi and F. Zamponi, Phys. Rev. Lett. **107**, 185702 (2011).
- [18] W. Götze, in *Liquids, Freezing and Glass Transition*, J.P. Hansen, D. Levesque, and J. Zinn-Justin, eds. (North-Holland, Amsterdam, 1991).
- [19] A. Andreanov, G. Biroli, and A. Lefèvre, J. Stat. Mech.:Theory Exp. P07008 (2006).
- [20] B. Kim and K. Kawasaki, J. Phys. A **40**, F33 (2007); J. Stat. Mech.:Theory Exp. P02004 (2008).
- [21] T.H. Nishino and H. Hayakawa, Phys. Rev. E **78**, 061502 (2008).
- [22] S.P. Das and G.F. Mazenko, Phys. Rev. A **34**, 2265 (1986).
- [23] W. Götze and L. Sjögren, Z. Phys. B **65**, 415 (1987).
- [24] R. Schmitz, J.W. Dufty and P. De, Phys. Rev. Lett. **71**, 2066 (1993).
- [25] G. F. Mazenko and J. Yeo, J. Stat. Phys. **74**, 1017 (1994).
- [26] M.E. Cates and S. Ramaswamy, Phys. Rev. Lett. **96**, 135701 (2006).
- [27] G. Szamel and H. Löwen, Phys. Rev. A **44**, 8215 (1991).
- [28] T. Gleim, W. Kob, and K. Binder, Phys. Rev. Lett. **81**, 4404 (1998).
- [29] G. Szamel and E. Flenner, Europhys. Lett. **67**, 779 (2004).
- [30] G. Szamel, Phys. Rev. Lett. **90**, 228301 (2003).
- [31] J. Wu and J. Cao, Phys. Rev. Lett. **95**, 078301 (2005).
- [32] P. Mayer, K. Miyazaki, and D.R. Reichman, Phys. Rev. Lett. **97**, 095702 (2006).
- [33] G. Szamel, AIP Conf. Proc. **982** 62 (2008).

-
- [34] G. Szamel, J. Chem. Phys. **127**, 084515 (2007).
 - [35] H.C. Andersen, J. Phys. Chem. B **106**, 8326 (2002).
 - [36] H.C. Andersen, J. Phys. Chem. B **107**, 10226 (2003).
 - [37] H.C. Andersen, in *Statistical Mechanics, Part A: Equilibrium Techniques*, B.J. Berne, ed. (Plenum, New York, 1977); J.-P. Hansen and I.R. McDonald, *Theory of Simple Liquids*, (Academic, London, 1986).
 - [38] W. Hess and R. Klein, Adv. Phys. **32**, 173 (1983).
 - [39] B. Cichocki and W. Hess, Physica A **141**, 475 (1987).
 - [40] K. Kawasaki, Physica A **215**, 61 (1995).
 - [41] G. Szamel, H. Hayakawa, E. Flenner, work in progress.
 - [42] S. Franz, H. Jacquin, G. Parisi, P. Urbani and F. Zamponi, arXiv:1206.2482.